Electronic Supplementary Material (ESI) for Nanoscale.

Supporting Information

Synthesis of sub-micrometer biphasic Au-AuGa$_2$ / Liquid Metal frameworks

Romain David* and Norihisa Miki

Department of Mechanical Engineering, Keio University, Yokohama 223-8522, Japan

Supplementary Figure FS1: (A) Standard and ice-bath sonication setups used for PVP-LM suspensions and Lys / NaAlg-LM suspensions respectively. (B) Evolution of the sonication bath temperature over the 15 min of sonication. (C) SEM pictures of GaO(OH) nanorods (left) and Lys-GaInSn spheres (right) formed with standard and ice bath sonication setups respectively, and their corresponding average composition (measured via EDX). As previously reported, the crystallization of the Lys-LM spheres is avoided at lower temperature using the ice bath setup (approx. 20°C).

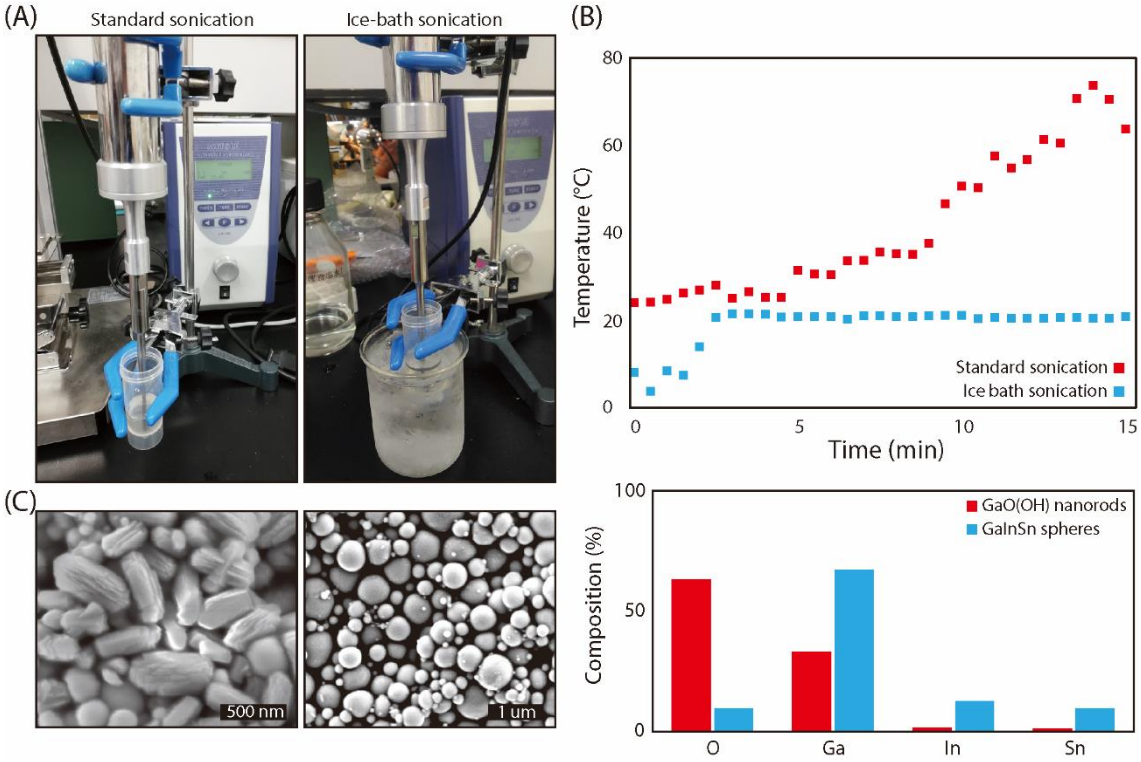

Supplementary Figure FS2: (A) FESEM pictures of an initial droplet after sonication without surfactant, or capped with lysozyme, PVP K25 or Na-alg 1.5% (scale bar = 1 um) (B) Composition of the initial droplets after sonication measured via EDX. Inset: atomic percentage of Na.

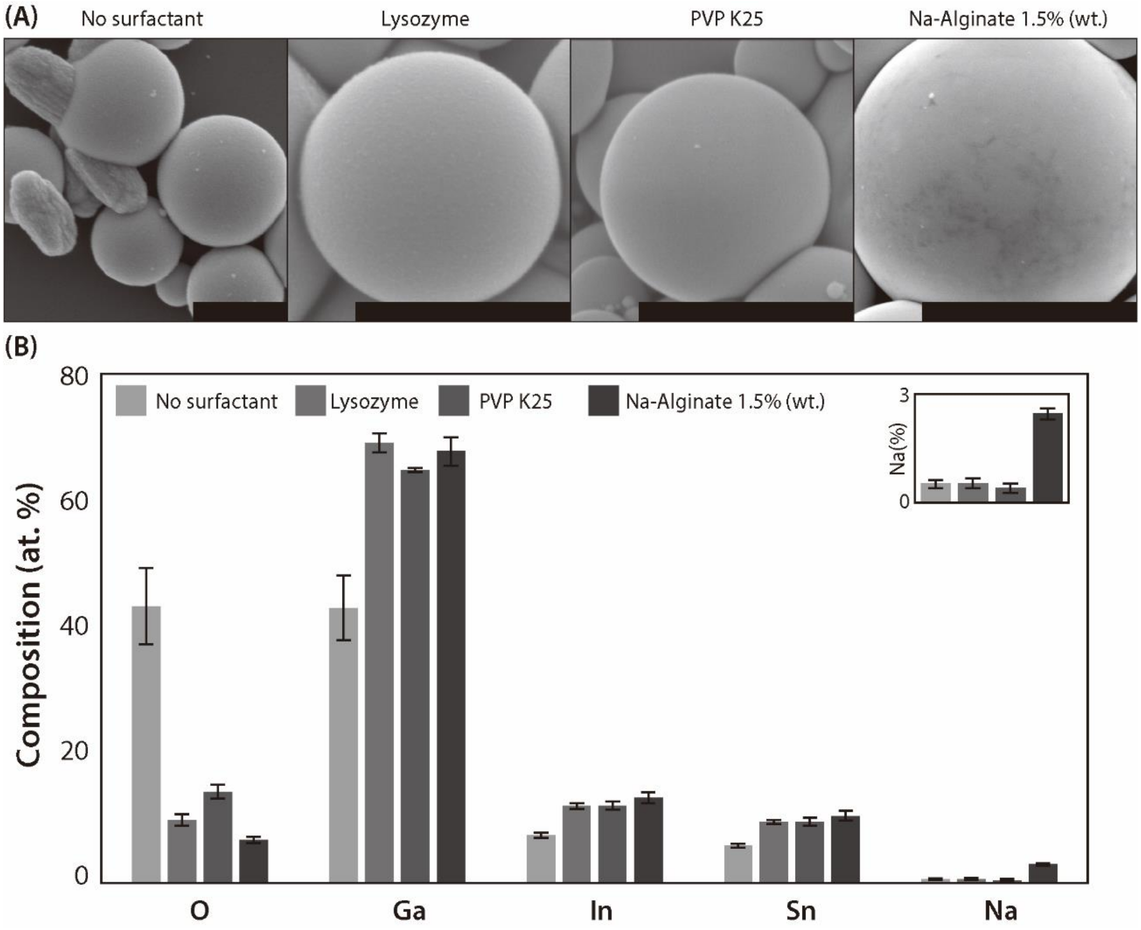

Supplementary Figure FS3: (A) Evolution over 72 h of the surface composition in O and Ga of the GaInSn droplets conserved in deionized water after sonication (measured via EDX). (B) SEM pictures of Lys-LM droplets taken at successive conservation times t = 0, 3, 24 and 72 hours. The morphological modification overtime in the form of oxidation and crystallization of the droplets is assessed. (scale bar = 10 um)

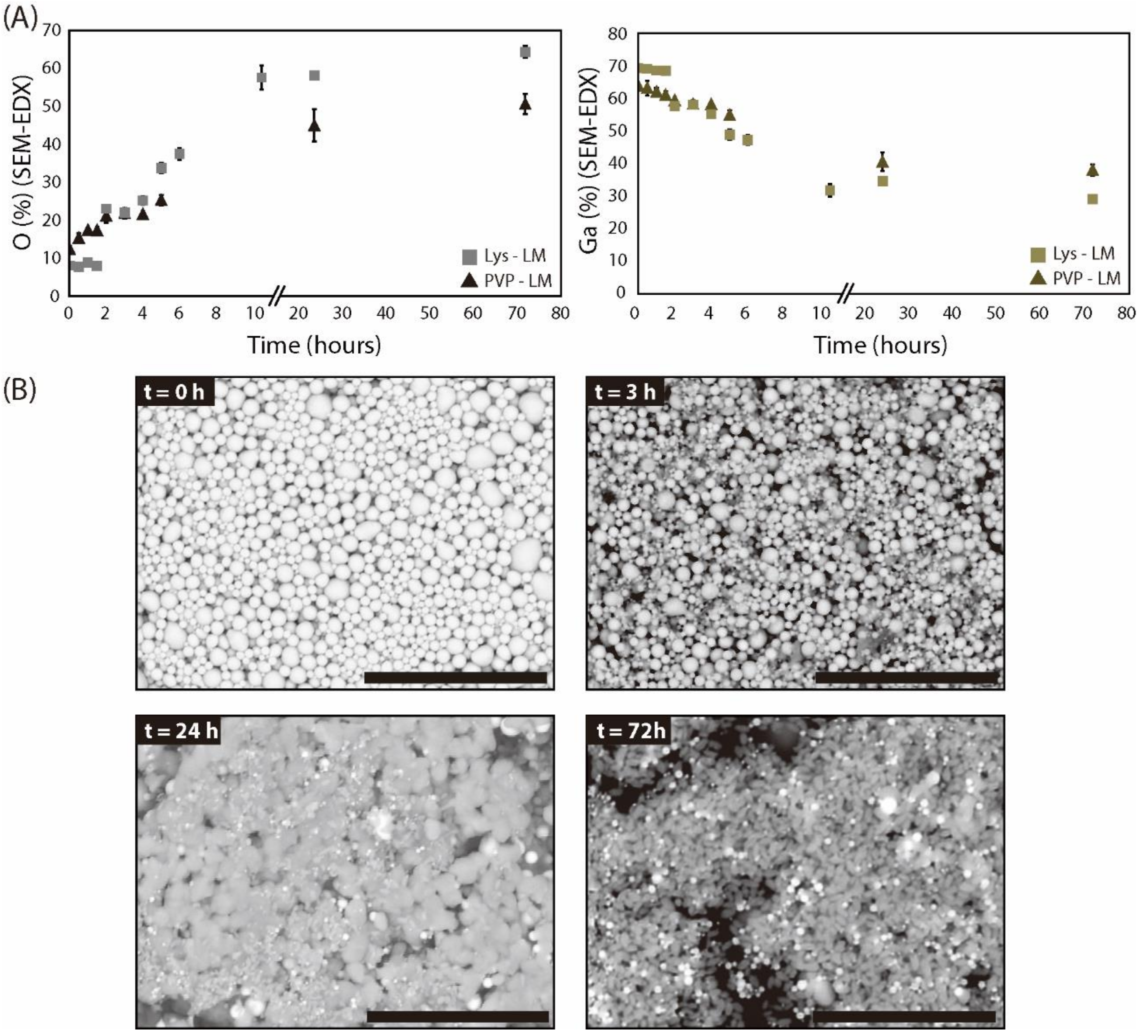

Supplementary Figure FS4: FE-SEM images of Au-LM droplets formed after 60 minutes in 10 mM $KAuBr_4$-KOH from Lys-LM suspension, presenting defects such as (A) partially encapsulation and (B) Au shell lift-off. These samples highlight the monolayered structure of the Au encapsulation, and allows an estimation of the encapsulation thickness via ImageJ-assisted measurements.

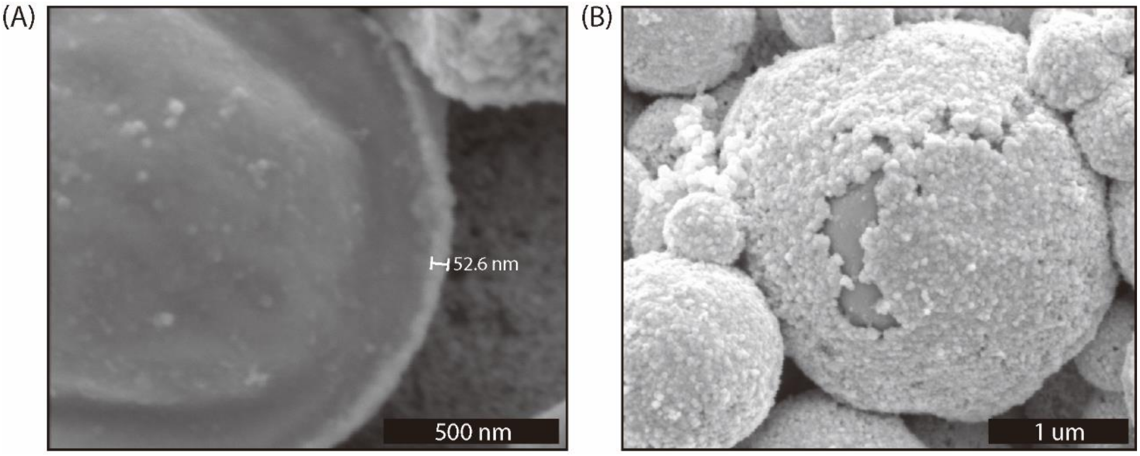

Table S5: EDX analysis of Au-Lys-LM frameworks formed in $KAuBr_4$ + KOH (at. %)

C(KAuBr4)	O (%)	Ga (%)	In (%)	Sn (%)	Au (%)	Na (%)	K (%)	Br (%)
0.5 mM	19.68	54.14	12.55	10.69	0.57	0	1.81	0.56
1 mM	24.29	46.78	14.35	12.06	2.08	0	1.78	0.65
2 mM	18.41	51.53	11.42	9.65	5.35	0	3.08	0.56
5 mM	18.11	43.50	12.66	10.60	12.62	0	2.20	0.38
10 mM	17.69	42.38	10.14	7.17	20.81	0	1.44	0.38

Table S6: EDX analysis of Au-Lys-LM frameworks formed in $KAuBr_4$ + NaOH (at. %)

C(KAuBr4)	O (%)	Ga (%)	In (%)	Sn (%)	Au (%)	Na (%)	K (%)	Br (%)
0.5 mM	16.49	56.22	12.64	11.25	0.63	0	2.07	0.69
1 mM	21.29	52.93	11.92	10.36	1.47	0	1.23	0.80
2 mM	13.04	54.24	13.50	11.48	4.27	0	3.01	0.46
5 mM	19.32	35.82	16.01	12.33	13.12	0	2.51	0.91
10 mM	18.11	39.45	11.49	9.08	18.47	0	1.91	1.08

Table S7: EDX analysis of Au-PVP-LM frameworks formed in $KAuBr_4$ + KOH (at. %)

C(KAuBr4)	O (%)	Ga (%)	In (%)	Sn (%)	Au (%)	Na (%)	K (%)	Br (%)
0.5 mM	18.33	57.84	12.47	9.69	1.04	0	0	0.64
1 mM	27.64	53.26	5.91	6.44	2.61	0	0.63	3.51
2 mM	21.48	47.94	10.46	8.67	8.63	0	1.99	0.84
5 mM	16.35	41.77	12.75	10.47	14.46	0	3.70	0.52
10 mM	38.25	27.63	5.47	3.97	23.68	0	0.86	0.15

Table S8: EDX analysis of Au-PVP-LM frameworks formed in $KAuBr_4$ + NaOH (at. %)

C(KAuBr4)	O (%)	Ga (%)	In (%)	Sn (%)	Au (%)	Na (%)	K (%)	Br (%)
0.5 mM	17.70	63.28	9.98	7.70	1.35	0	0	0
1 mM	19.91	42.82	9.28	7.73	2.48	0	1.31	0
2 mM	22.35	49.05	11.26	8.73	6.12	0	2.51	0.02
5 mM	18.58	47.96	7.82	6.62	14.29	0	2.91	1.91
10 mM	19.69	40.99	7.51	5.83	24.42	0	1.21	0.31

Table S9: EDX analysis of Au-NaAlg-LM frameworks formed in $KAuBr_4$ + KOH (at. %)

C(KAuBr4)	O (%)	Ga (%)	In (%)	Sn (%)	Au (%)	Na (%)	K (%)	Br (%)
1 mM	16.70	48.29	16.29	12.98	1.76	0	2.31	0.52
5 mM	20.90	46.96	11.70	10.00	7.86	0	2.20	0.38
10 mM	39.29	21.27	6.02	5.43	22.21	0	3.22	0.91

Supplementary Figure FS10: (A) FESEM picture of a local Au nanoparticles lift-off on Au-LM droplets formed after 60 min reaction in 10 mM $KAuBr_4$-KOH from Lys-LM suspension, exposing the underlying interfacial surface between the nanoparticles and the liquid metal core outer surface. (B) EDX measurements of the shell and exposed interfacial surface

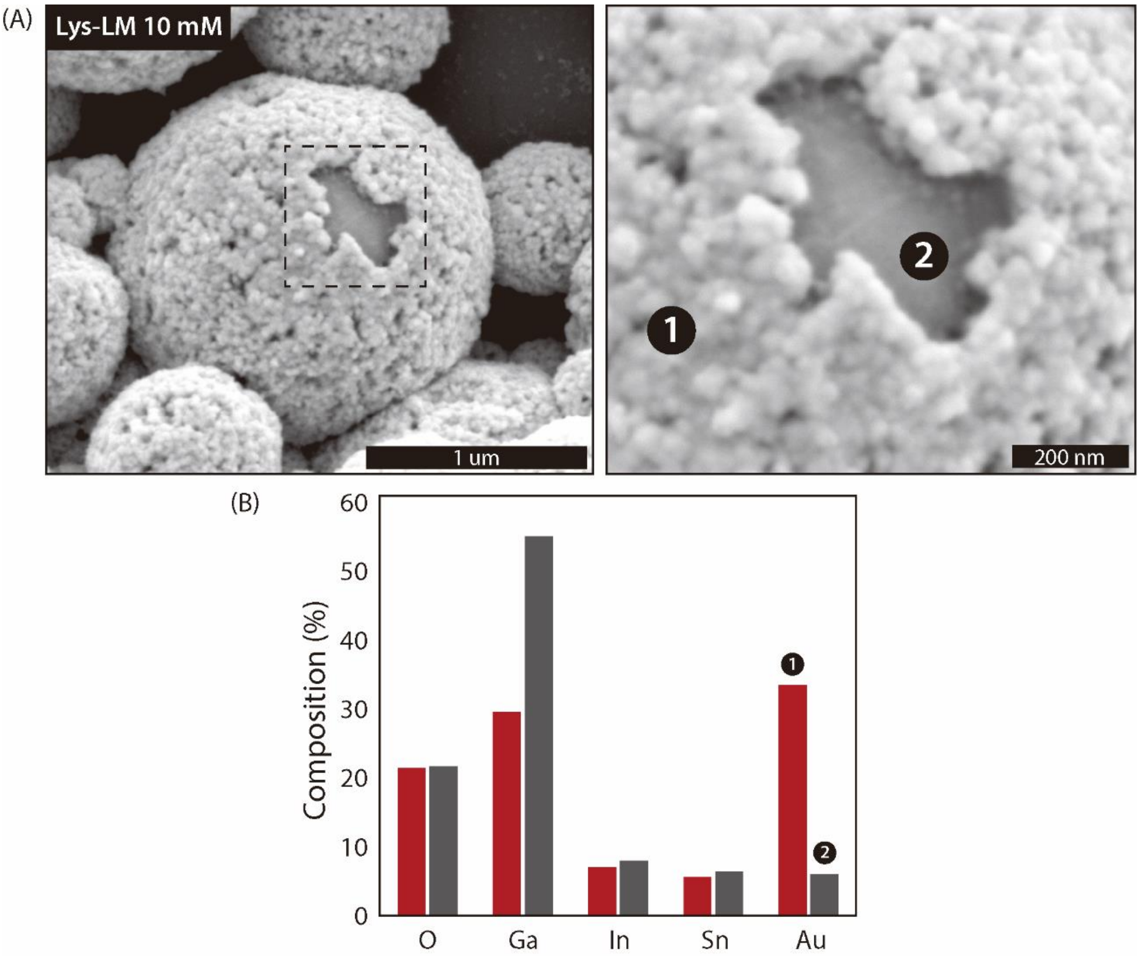

Supplementary Figure FS11: (A) Optical pictures of mechanically sintered NaAlg-LM, Lys-LM and PVP-LM samples after galvanic replacement in 1, 5 and 10 mM alkaline $KAuBr_4$ solutions (scale bar = 100 um). Mechanical sintering was conducted with a stainless steel tool. (B) Low and high magnification SEM pictures of the mechanically sintered PVP-LM samples (scale bars = 100 and 5 um respectively).

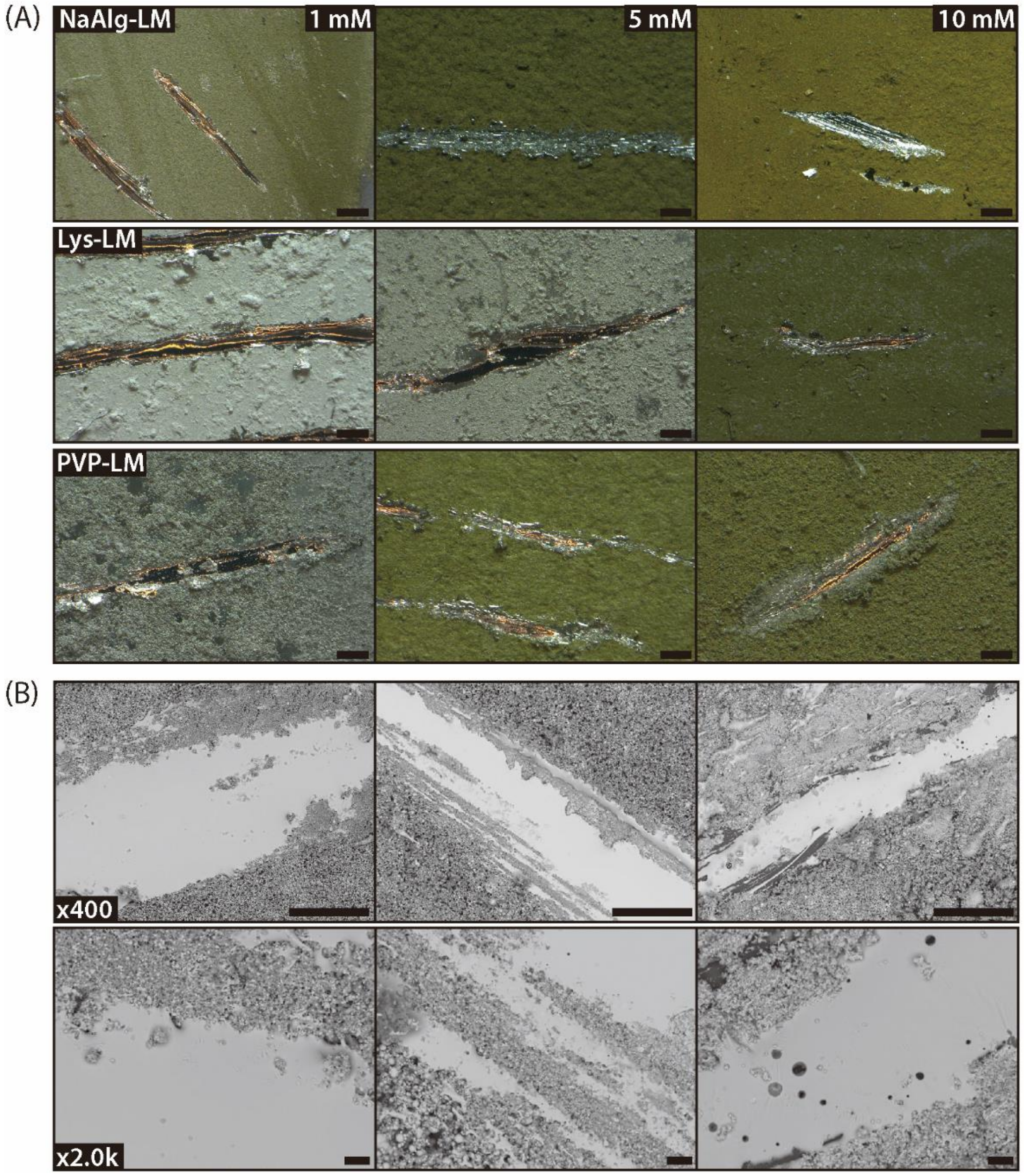

Supplementary Figure FS12: (A) SEM pictures of PVP-LM (left) and NaAlg-LM (right) after galvanic replacement in acidic 10 mM $KAuBr_4$ solution for 1 hour. While solid Au is visible on the structures, the initial morphology of the LM particles is lost during the reaction, due the oxidation occurring in acidic pH. (scale bars = 10 um) (B) EDX mapping in Ga and Au of Lys-LM after galvanic replacement in acidic 10 mM $KAuBr_4$ solution for 1 hour, confirming the complete uniformity of the process in acidic conditions. (C) EDX measurements of the frameworks formed with PVP and Lys in acidic medium. (D) XRD of the structures formed with PVP-LM and Lys-LM in acidic $KAuBr_4$. Compared to alkaline solutions, the Au peaks intensity is relatively low.

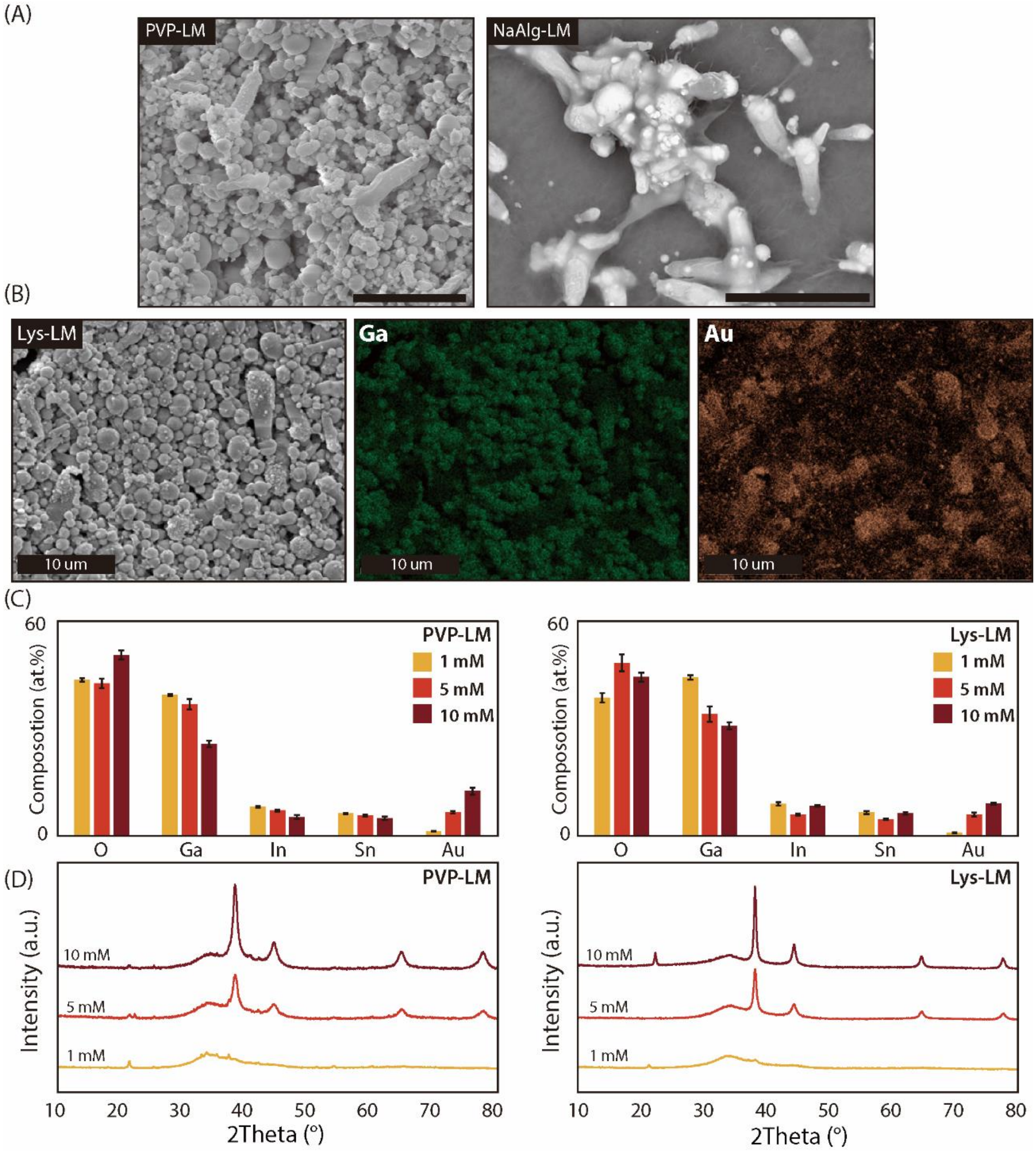

Supplementary Figure FS13: XRD spectra of Au-PVP-LM and Au-Lys-LM formed in 1, 5 and 10 mM alkaline $KAuBr_4$ tuned with NaOH.

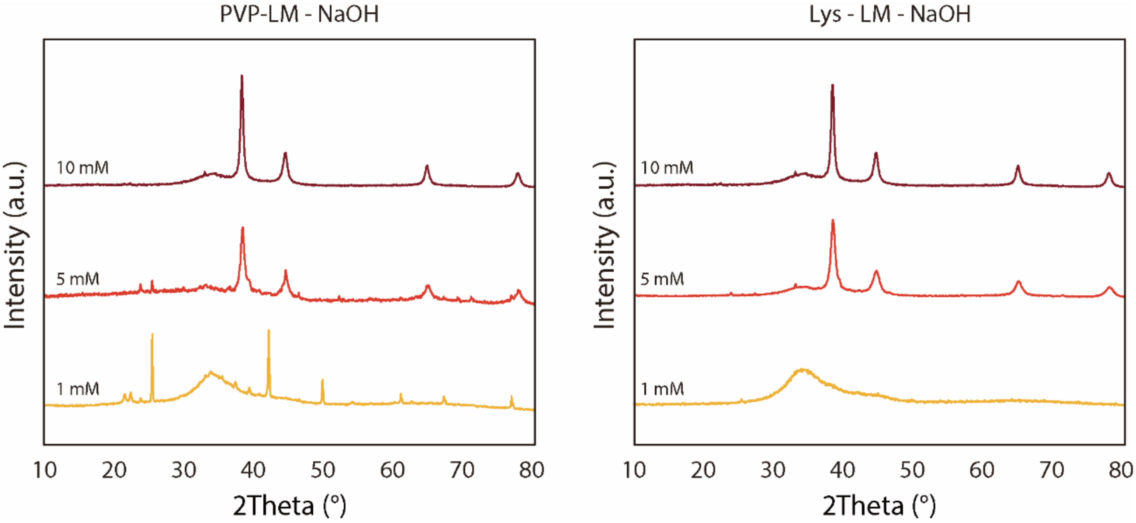

Supplementary material S14: Relation between galvanic replacement and evolution of the pH

The galvanic replacement of Ga-alloys in $KAuBr_4$ was shown to be dominated by the oxido-reduction reaction between Ga(s) and $AuBr_4^-$ anion:[2]

$$\mathrm{Ga^0{}_{(s)} + AuBr_4^-{}_{(aq)} \rightarrow Ga^{3+}{}_{(aq)} + Au^0{}_{(s)} + 4Br^-{}_{(aq)}} \quad (1)$$

Depending on the pH of the solution in which the galvanic replacement takes place, the released Ga3+ cations will either be stable or react, following the Eh-pH stability domains of Ga-species in aqueous solutions.[3] If the pH is below 3, the Ga^{3+} cations are stable. However, if the pH is above 3, the cations are reduced into Ga_2O_3 oxide.

$$\mathrm{2Ga^{3+}{}_{(aq)} + 3H_2O \leftrightarrow Ga_2O_3{}_{(s)} + 6H^+} \qquad (2)$$

If the pH is above 11.7, the Ga_2O_3 oxide is further reduced into GaO_3^{3-}:

$$\mathrm{Ga_2O_3}{}_{(s)} + \mathrm{3H_2O} \rightarrow \mathrm{2GaO_3^{3-}}{}_{(aq)} + \mathrm{6H^+} \qquad (3)$$

Then, by summarizing the successive reactions following the galvanic replacement reaction (1), we can isolate two separate cases depending on the value of the pH:

For pH > 11.7 $\mathrm{2Ga^0{}_{(s)} + 2AuBr_4^-{}_{(aq)} + 3H_2O \leftrightarrow 2Au^0{}_{(s)} + 8Br^-{}_{(aq)} + 2GaO_3^{3-}{}_{(aq)} + 12H^+}$

For 11.7 > pH > 3 $\mathrm{2Ga^0{}_{(s)} + 2AuBr_4^-{}_{(aq)} + 3H_2O \leftrightarrow 2Au^0{}_{(s)} + 8Br^-{}_{(aq)} + Ga_2O_3{}_{(s)} + 6H^+}$

The reaction rate of the galvanic replacement in initially alkaline solution can then be directly determined from the decrease of the pH upon release of protons.

Additionally, if we consider the LM suspensions as neutral aqueous solutions, the pH decrease due to the addition of 1.5 mL to the 4 mL of alkaline $KAuBr_4$ of initial $pH_i > 11.7$ can be considered as a simple dilution decrease:

$$\triangle\, pH = log_{10}\left(\frac{4}{5.5}\right) \# \; 0.14$$

Thus, the pH decrease caused by the addition of the LM suspension before start of the reaction is entirely negligible.

Supplementary Figure FS15: Pictures of the initial 10 mM $KAuBr_4$ solution, the alkaline $KAuBr_4$-KOH solution, the solution at the start of the reaction, and the supernatant before and after isolation after 60 min of reaction. The colorless supernatant indicates the total consumption of the initially present $AuBr_4^-$ ions.

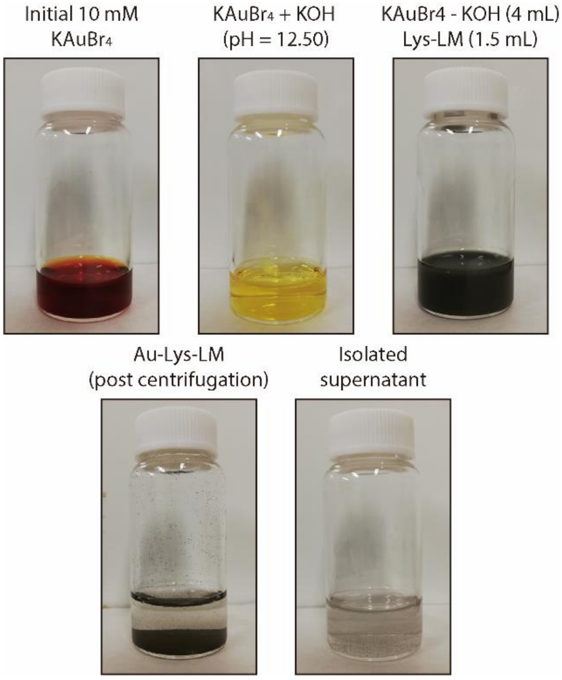

Supplementary Figure FS16: pH evolution during galvanic replacement of PVP-LM and Lys-LM in $KAuBr_4$ tuned with NaOH. The pH decrease trend is identical to the one observed for reaction in $KAuBr_4$ tuned with KOH.

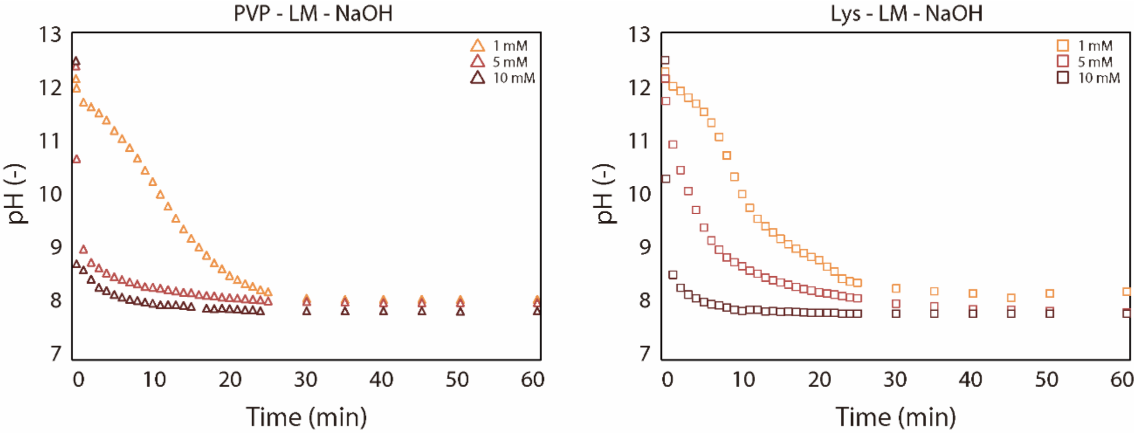

Supplementary Figure FS17: (A) Reaction kinetics and resulting XRD structures of Au-PVP-LM after galvanic replacement in alkaline 10 mM $KAuBr_4$ tuned with KOH to an initial pH of 12.50 and 13.05 respectively. For pH_{ini} = 12.50, fast pH decrease is observed, leading to AuNPs formed on the LM spheres, as seen on XRD spectrum on SEM observations. However, for pH_{ini} = 13.05, the kinetic of the reaction is drastically slowed, leading to the formation of $AuGa_2$ instead on the LM spheres, which further confirms the direct correlation between reaction kinetics and crystal structure. (B) In the case of pH_{ini} = 13.05, colloidal AuNPs were obtained in solution, as conserved by the presence of an absorbance peak at 524 nm, which is characteristic of the surface plasmon resonance of gold nanoparticles.

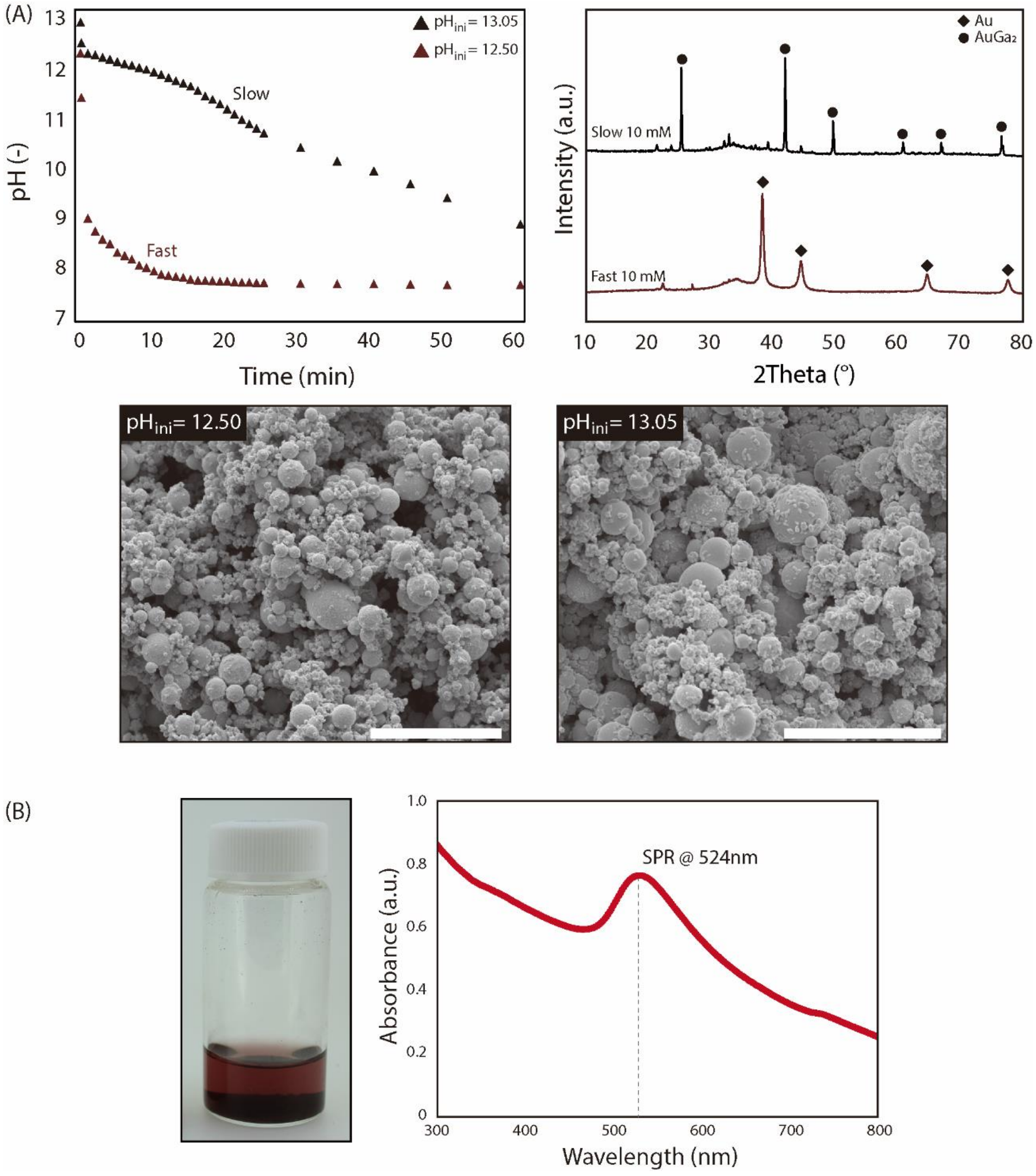

Supplementary Figure FS18: XRD spectra at t = 0, 2 and 4 weeks of Au-PVP-LM and Au-NaAlg-LM frameworks formed in 10 mM $KAuBr_4$-KOH and Au-PVP-LM and Au-Lys-LM frameworks formed in 1 and 5 mM alkaline $KAuBr_4$-KOH. The invariance of the XRD spectra confirms the structural and chemical stability of the Au-LM frameworks overtime in dry environment, as seen on FESEM observations at t = 4 weeks.

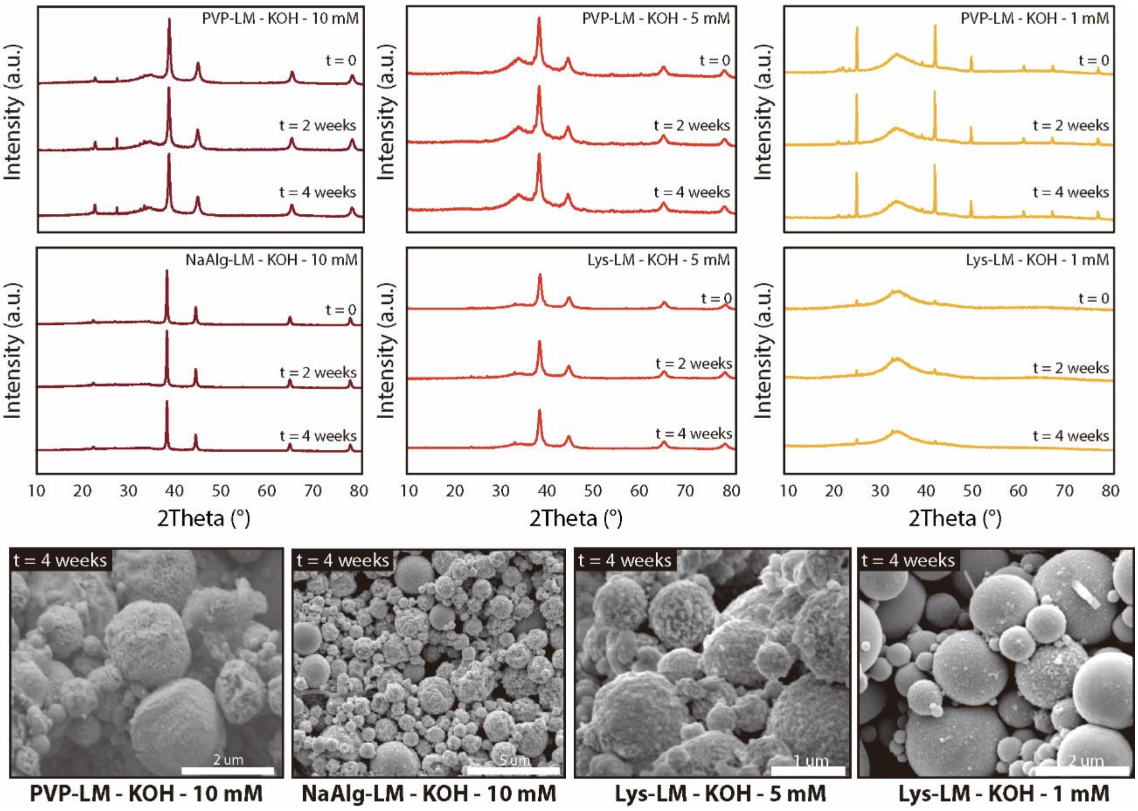

Supplementary Figure FS19: Front and back side of Lys-LM deposited on borosilicate glass after galvanic replacement in 1 and 10 mM alkaline $KAuBr_4$ tuned with KOH for 15 min. While the front side exposed to the solution is modified, the backside remained unreacted.

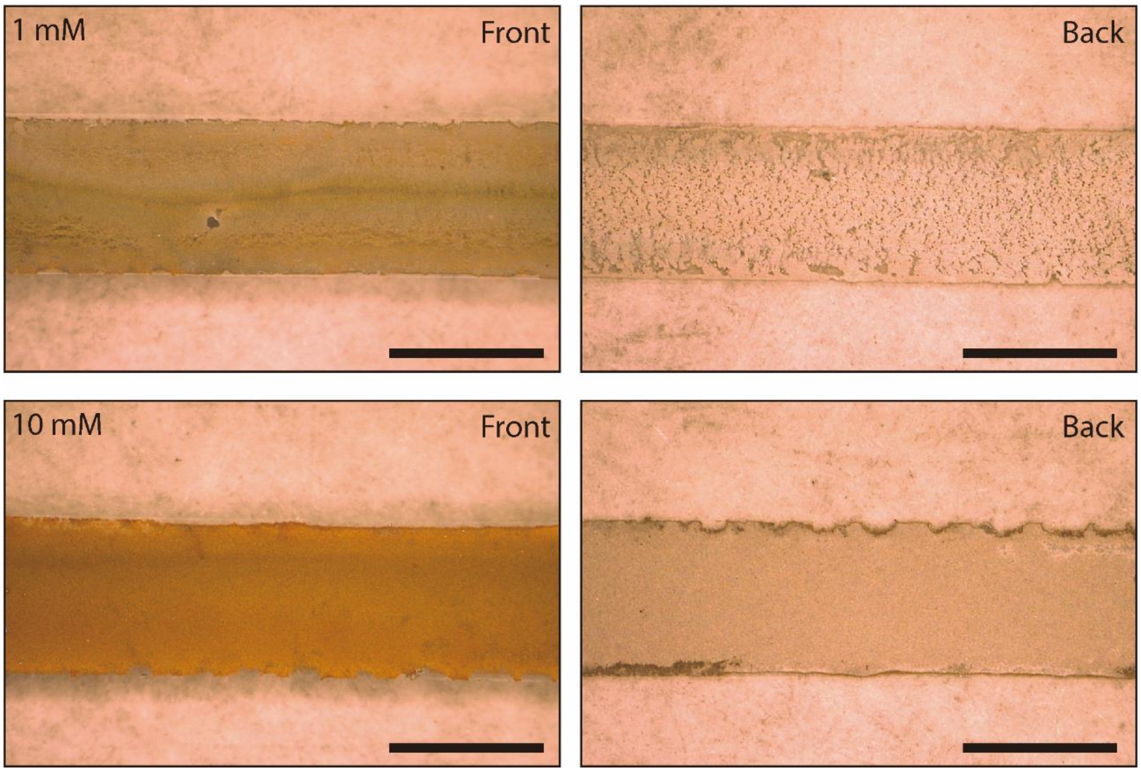

Supplementary Figure FS20: (A) EDX mapping in Au and Ga of the top surface of Lys-LM deposited on glass after galvanic replacement in 1 and 10 mM alkaline $KAuBr_4$, (B) the corresponding average composition measured and (C) XRD spectra. (scale bars = 1 um)

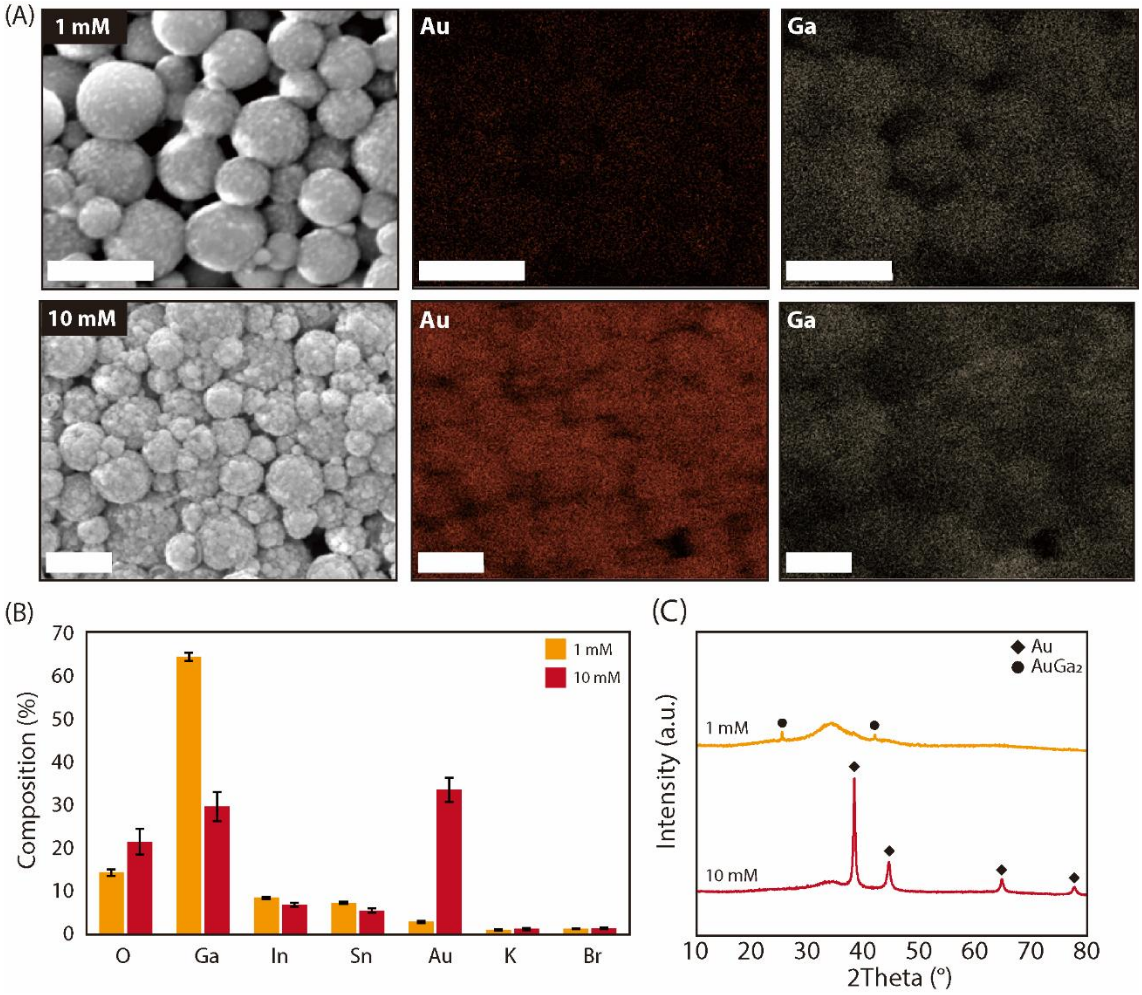

Supplementary Figure FS21: (A) XRD spectra of frameworks formed on LM droplets without surfactant or capped with PVP, Lys or Na-Alg after galvanic replacement with 1, 5 and 10 mM $KAuBr_4$-KOH for 10 minutes and (B) FESEM pictures of the single droplets after the encapsulation reaction (scale bar = 1 um)

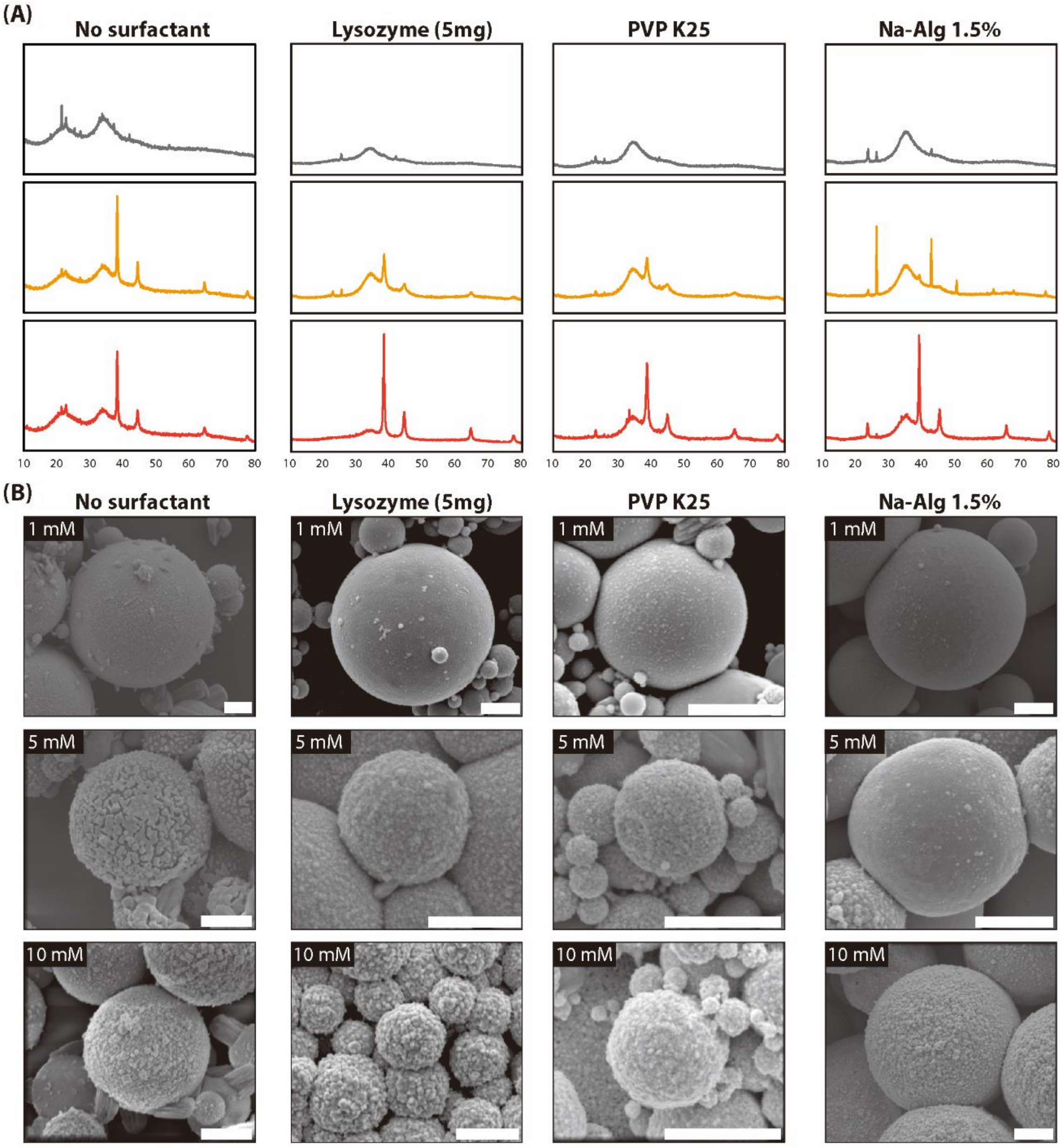

Supplementary Figure FS22: (A) FESEM pictures of the top surface of Lys-LM deposited on borosilicate glass after galvanic replacement in 1 and 10 mM alkaline $KAuBr_4$ at t = 0, 10 and 40 days. (B) The corresponding XRD spectra of the 1 mM and 10 mM samples at t = 0, 10 and 40 days.

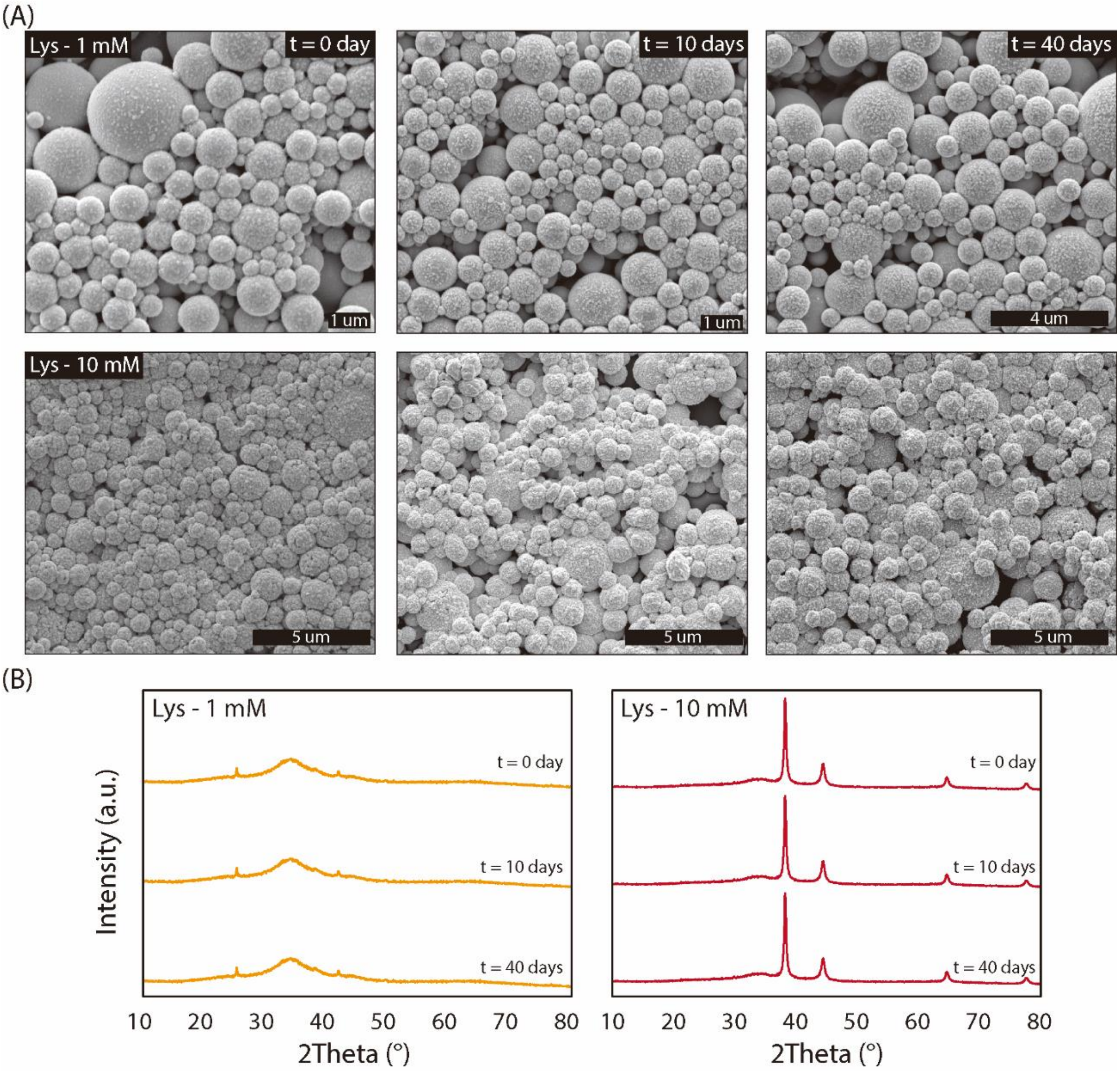

Supplementary Figure FS23: (A) Picture of the 2-probe measurement setup for conductivity measurement on Au/$AuGa_2$-LM films. (B) Conductivity of LM, $AuGa_2$-LM and Au-LM lines formed on borosilicate glass slides

(A)

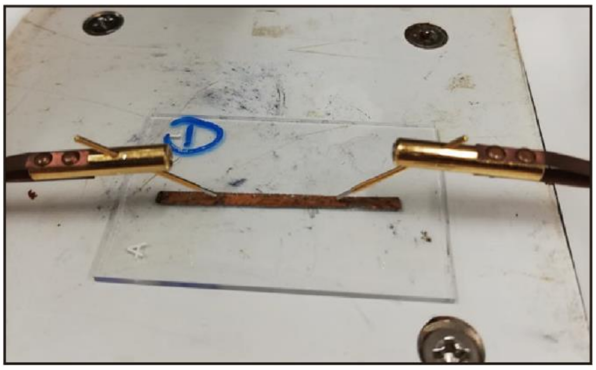

(B)

Reaction medium	**Reaction time**	**Conductivity**
-	-	Non-conductive
1 mM KAuBr4 + KOH	Any	Non conductive
10 mM reaction + KOH	Above 1’	Conductive

Supplementary Figure FS24: Evolution over 30 days of the resistance of the Au-LM films on borosilicate glass formed with 10 mM $KAuBr_4$ tuned with KOH for reaction times of 10, 15, 30 and 45 min.

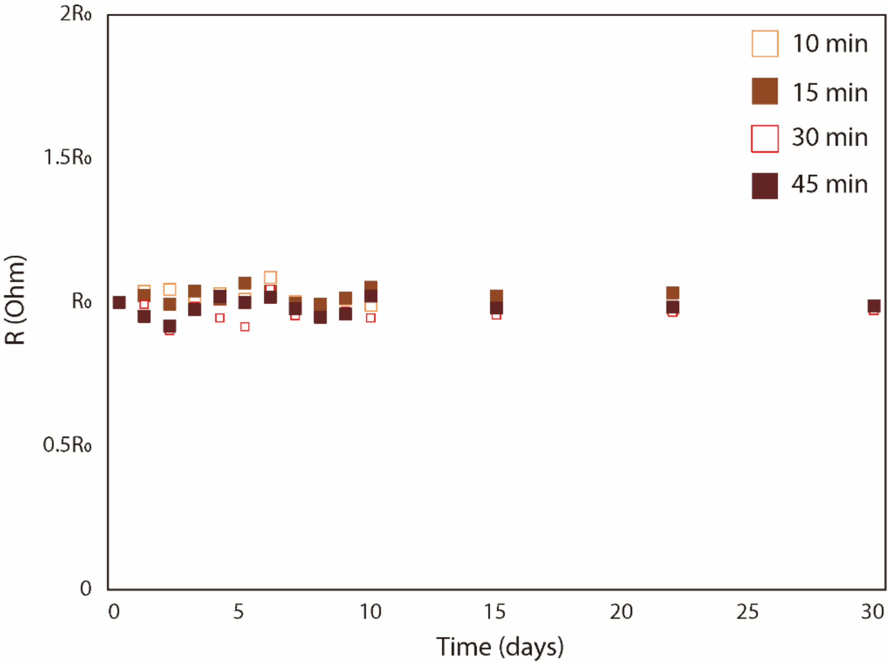

Supplementary Figure FS25: (A) (A) EDX mapping in Au and Ga of the top surface of C12-LM suspension in 2-propanol deposited on glass, after galvanic replacement in 1 and 10 mM alkaline $KAuBr_4$ for 10 minutes, (B) the corresponding average composition measured and (C) XRD spectra. (scale bars = 2 um)

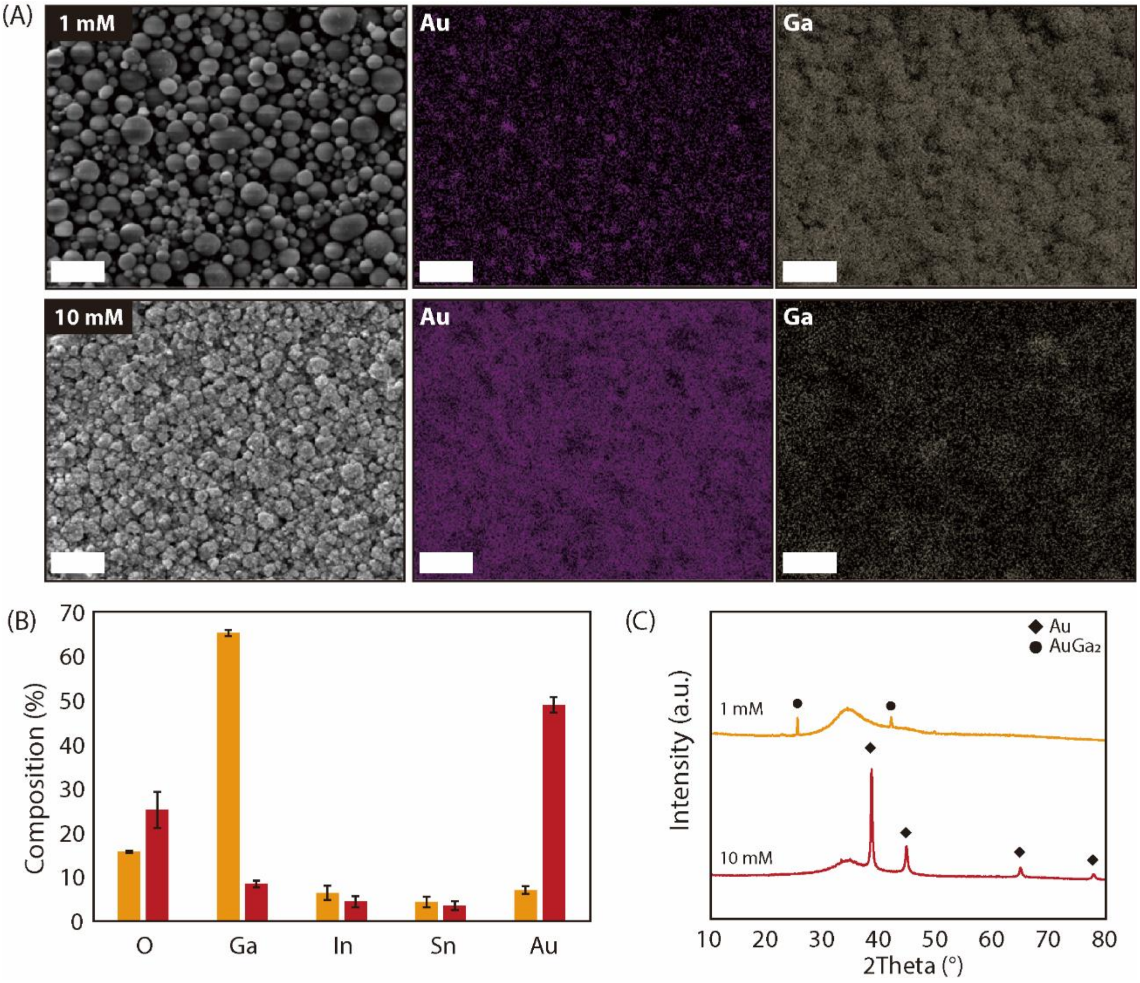

Supplementary Figure FS26: Scaling-down of the frameworks formed from ethanolic suspensions of GaInSn. (A) Average diameter of the LM droplets with sonication time (power = 210W). (B) EDX measurement in Au (at.%) on the surface of the frameworks for a reaction time of 10 minutes at a given $KAuBr_4$-KOH concentration. (C) FESEM picture of the initial LM droplets, and of single droplet after galvanic replacement reaction. (D) XRD spectra of the frameworks.

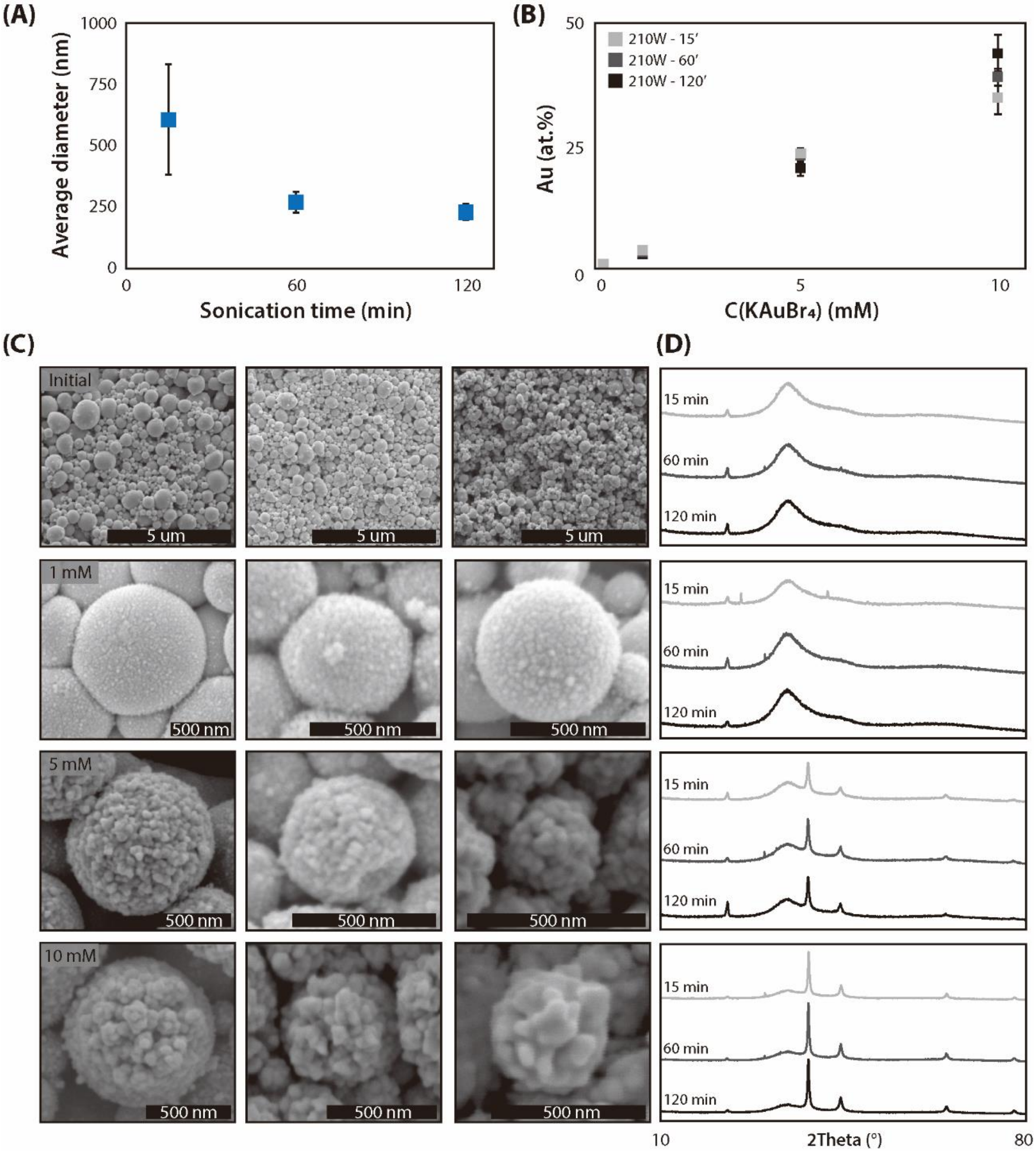

Supplementary Figure FS27: SEM observation and EDX measurements of the composition of the initial droplets and sintered lines for (A) initial C12-GaInSn and (B) Au-C12-GaInSn formed after GRR for 10 min in 10 mM $KAuBr_4$-KOH. The EDX measurements reveal the composition of the sintered line is dependent to the initial composition of the droplets in Au. The LM lines are conductive after mechanical sintering regardless of the initial droplet composition

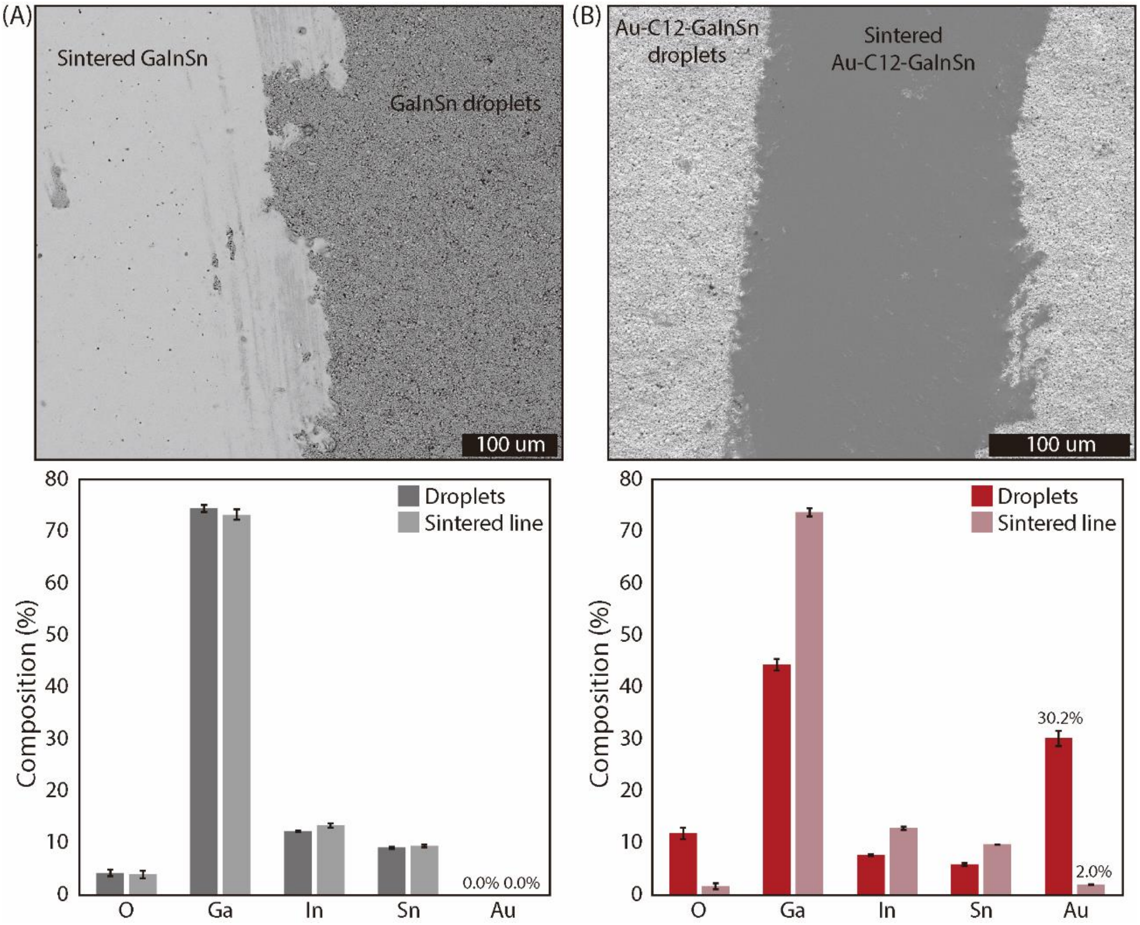

	Before sintering	**After sintering**
C12-GaInSn-IPA	Non-conductive	1.6 ± 0.1 Ω
Au-C12-GaInSn-IPA	20.7 ± 1.2 Ω	1.26 ± 0.2 Ω

Supplementary Figure FS28: (A) Design of the Ni-stencil used for micro-patterning of the LM surfaces. (B) Au micro-patterns of width ranging from 500 to 30 um formed on Lys-LM deposited on borosilicate glass after 10 min galvanic replacement with a 10 mM alkaline $KAuBr_4$+KOH. (scale bars = 1 mm)

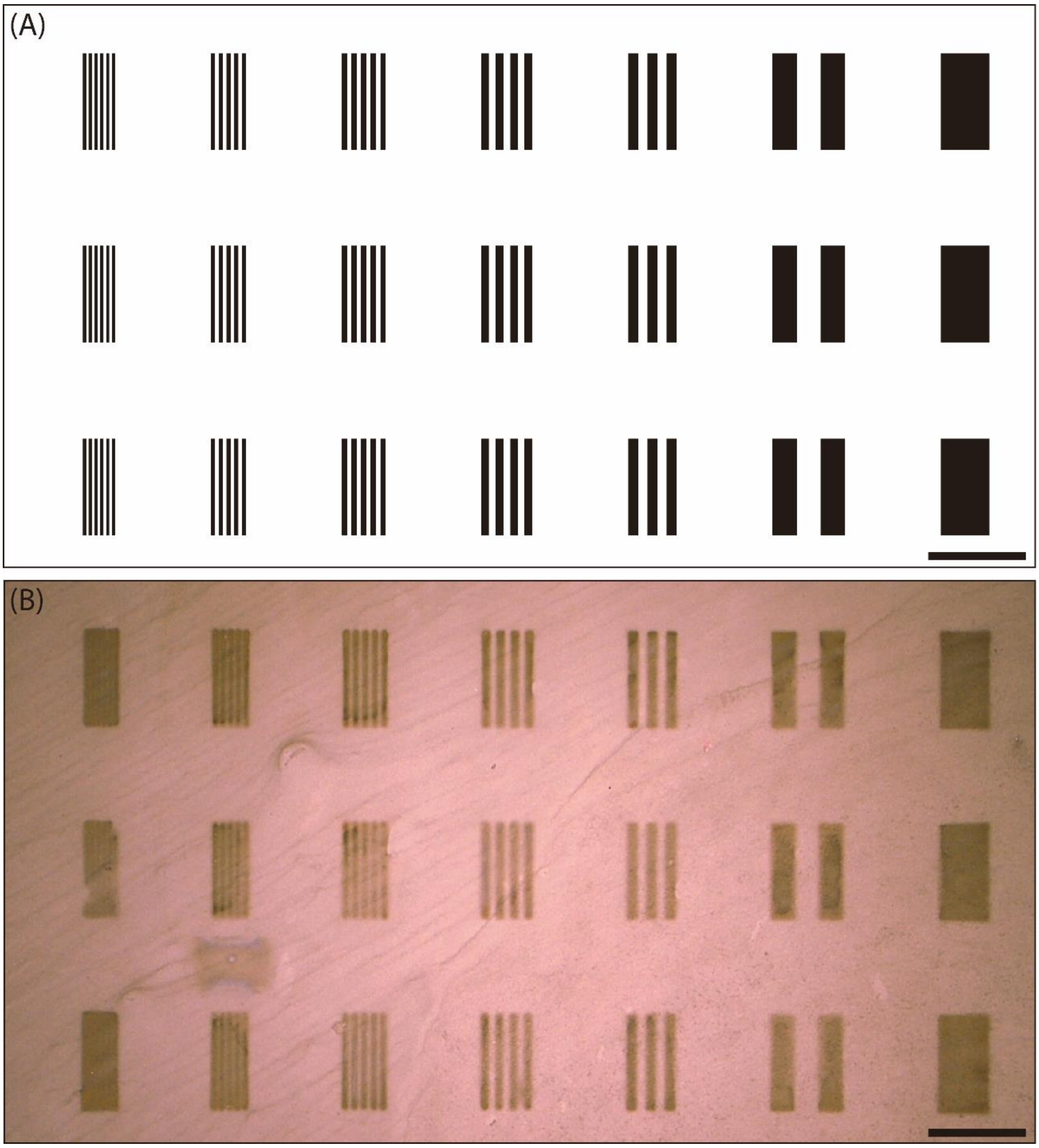

Supplementary Figure FS29: SEM pictures and EDX mapping in Au of the 50 um patterns formed with (A) 1 mM and (B) alkaline $KAuBr_4$. The structure of the encapsulation, $AuGa_2$ or Au, is similar to those of previous samples formed in 1 and 10 mM respectively.

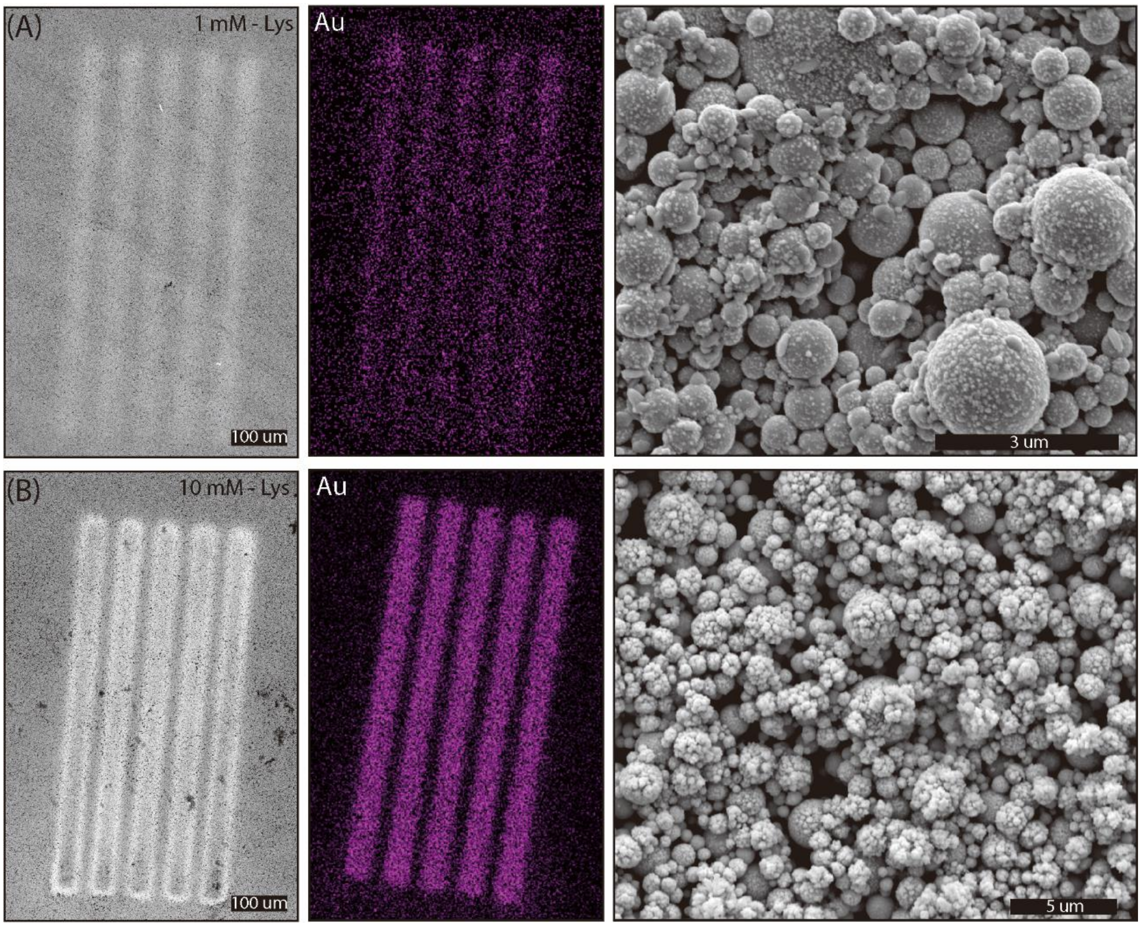

Supplementary Figure FS30: (A) Dimensional ratio of the patterns formed in 1 and 10 mM alkaline $KAuBr_4$ on Lys-LM and PVP-LM. (B) Evolution of the amount of Au on the patterns and $Au_{(l)}$ between the patterns $Au_{(p)}$ with the width of the stencil slits. Smaller slit and spacing widths leads to higher amount of Au between the patterns.

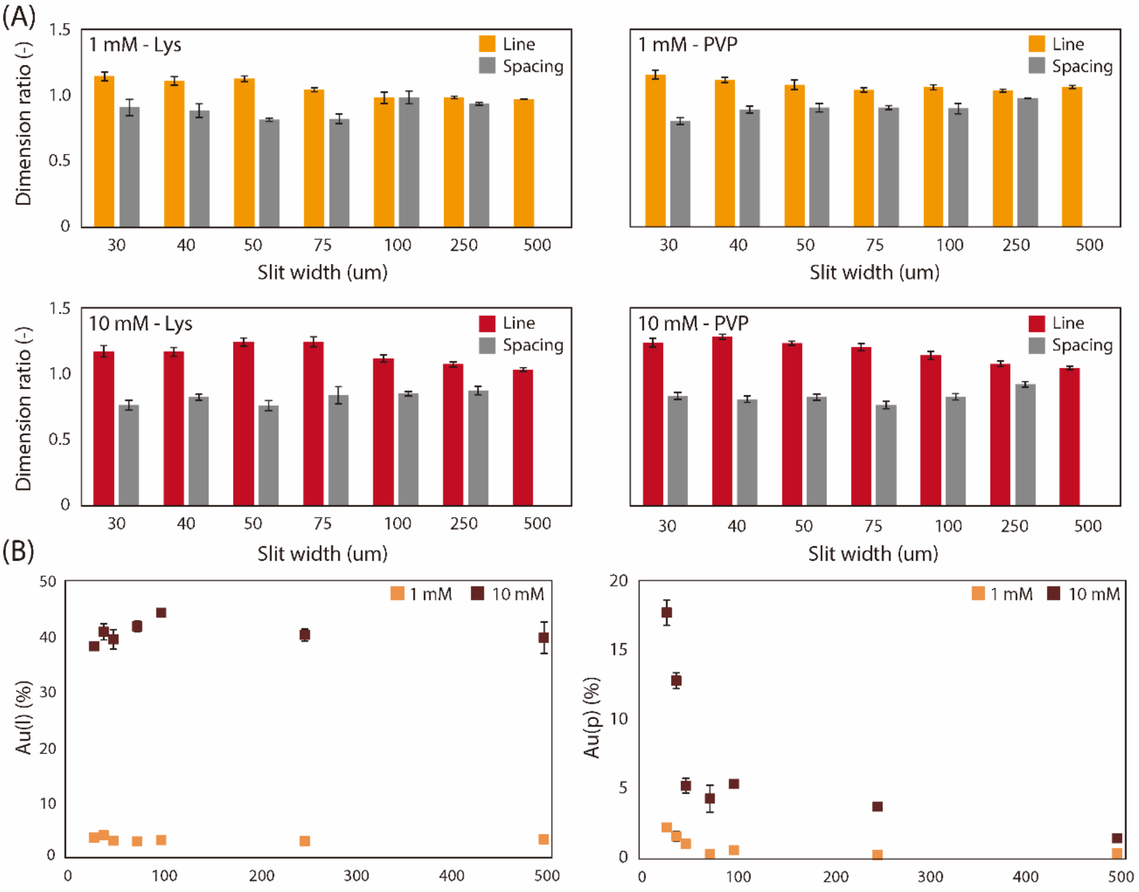

Supplementary Figure FS31: EDX profile in Au across the patterned lines obtained in 10 mM $KAuBr_4$ tuned with KOH for a width of (A) 250 (B) 100 (C) 50 and (D) 30 um. The amount of Au in the spacing between adjacent lines increases with smaller spacing.

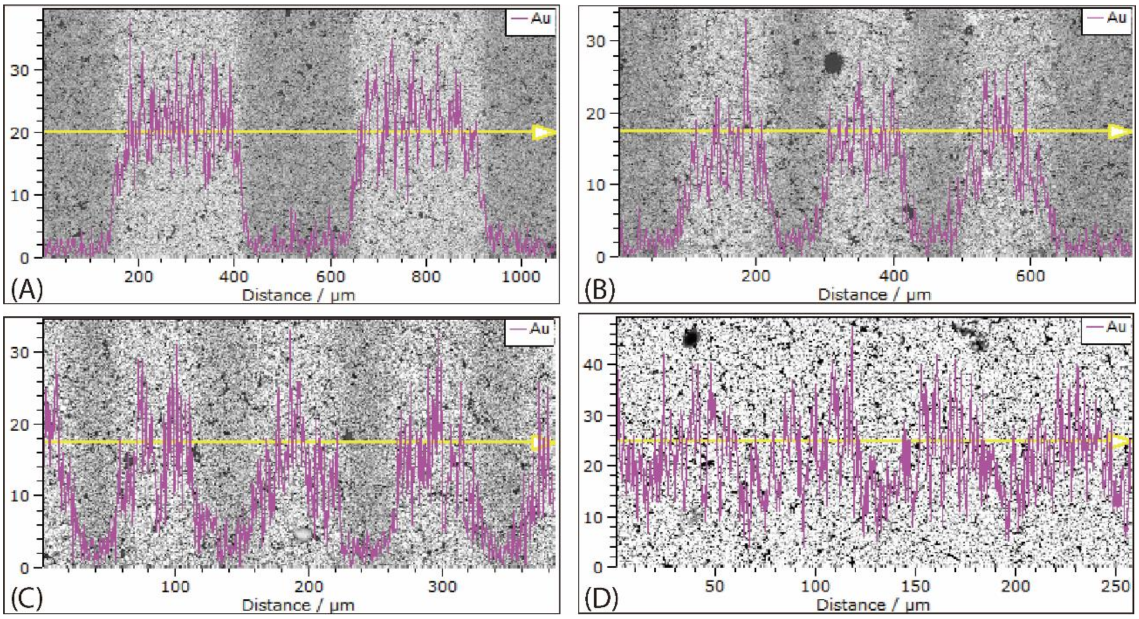

Supplementary Figure FS32: Galvanic replacement through a 500 um pattern through an AZ photoresist stencil formed via standard photolithography process (scale bar = 500 um). While galvanic replacement occurs on the exposed droplets only, the use of highly alkaline solvent during the strip-off step leads to the partial dissolution and coalescence of the LM droplets, as seen on the SEM picture.

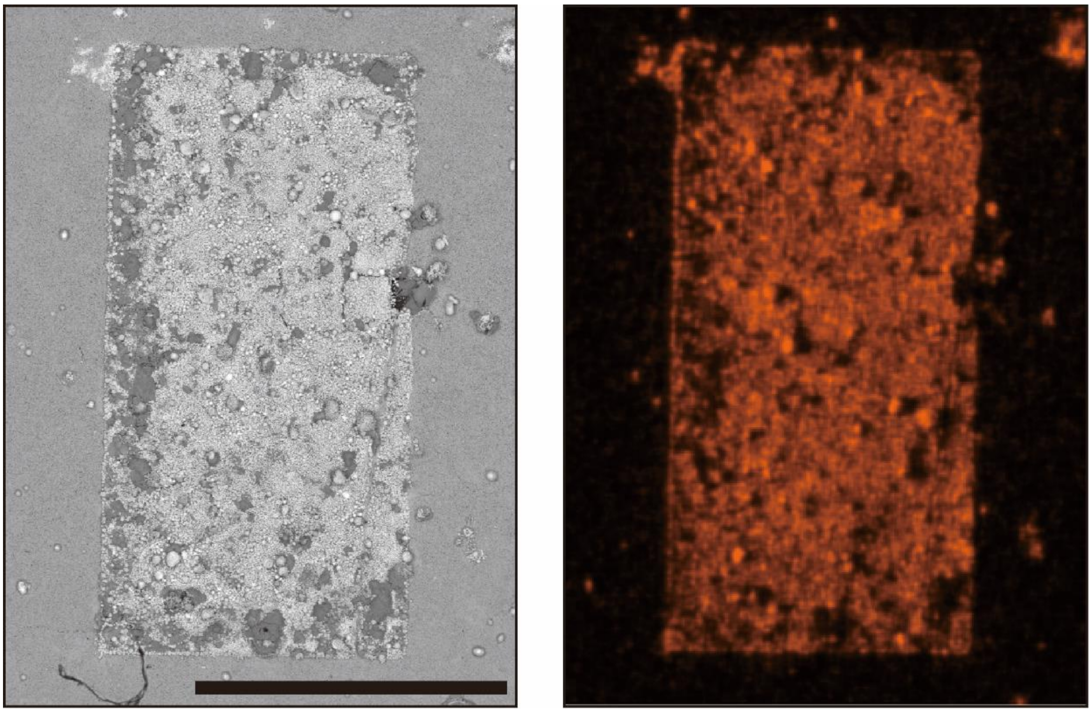

Supplementary Figure FS33: Optical pictures of the Au-MoM-LM droplets before and after dipping in deionized water (top) and 1 M NaOH solution (bottom). (scale bar = 500 um)

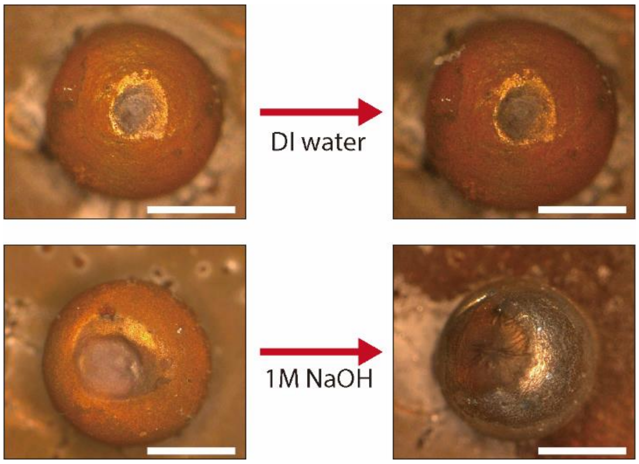

Supplementary Figure FS34: (A) The PMMA phase drop chip. Channels to hold the two carbon electrodes, the saline buffer and the droplet socket were milled in the PMMA chip. The two carbon electrodes are connected to a LCR impedance analyzer. (B) The equivalent electrical circuit of the phase drop chip. The impedance of the socket varies with its content. Details on the equivalent electrical circuit and the theoretical considerations of the measure were previously discussed.[4]

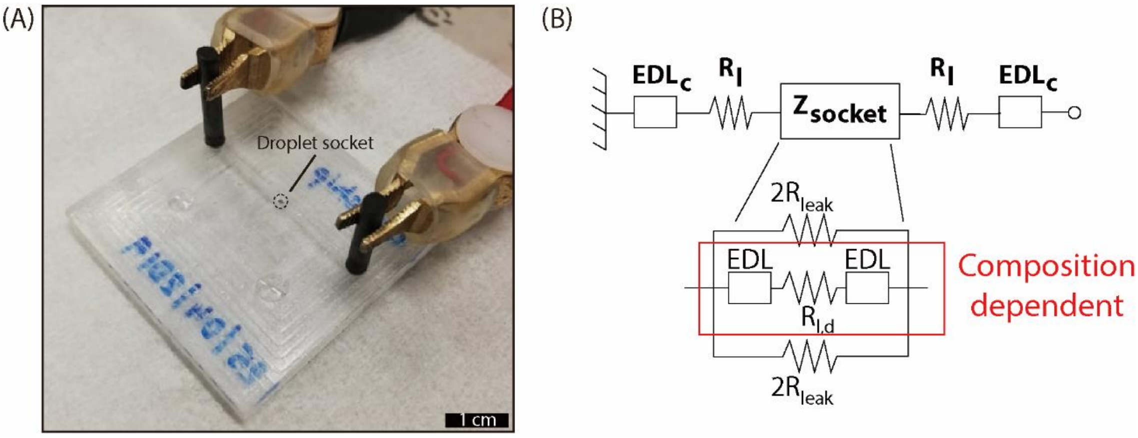

References

(1) Daeneke, T.; Khoshmanesh, K.; Mahmood, N.; de Castro, I. A.; Esrafilzadeh, D.; Barrow, S. J.; Dickey, M. D.; Kalantar-zadeh, K. Liquid Metals: Fundamentals and Applications in Chemistry. *Chem. Soc. Rev.* **2018**, *47* (11), 4073–4111. https://doi.org/10.1039/C7CS00043J.

(2) Hoshyargar, F.; Crawford, J.; O’mullane, A. P. Galvanic Replacement of the Liquid Metal Galinstan. *J. Am. Chem. Soc* **2017**, *139*, 1464–1471. https://doi.org/10.1021/jacs.6b05957.

(3) Takeno, N. *Atlas of Eh-PH Diagrams Intercomparison of Thermodynamic Databases*; 2005.

(4) David, R.; Miki, N. Tunable Noble Metal Thin Films on Ga Alloys via Galvanic Replacement. *Langmuir* **2018**, *34* (36), 10550–10559. https://doi.org/10.1021/acs.langmuir.8b02303.